

GALAXY-GALAXY FLEXION: WEAK LENSING TO SECOND ORDER

DAVID M. GOLDBERG & DAVID J. BACON

DEPARTMENT OF PHYSICS, DREXEL UNIVERSITY, PHILADELPHIA, PA 19104 ; INSTITUTE FOR
ASTRONOMY, SCHOOL OF PHYSICS, UNIVERSITY OF EDINBURGH, ROYAL OBSERVATORY,
EDINBURGH, EH9 3HJ, U.K.

Draft version August 26, 2018

ABSTRACT

In this paper, we develop a new gravitational lensing inversion technique. While traditional approaches assume that the lensing field varies little across a galaxy image, we note that this variation in the field can give rise to a “Flexion” or bending of a galaxy image, which may then be used to detect a lensing signal with increased signal to noise. Since the significance of the Flexion signal increases on small scales, this is ideally suited to galaxy-galaxy lensing. We develop an inversion technique based on the “Shapelets” formalism of Refregier (2003). We then demonstrate the proof of this concept by measuring a Flexion signal in the Deep Lens Survey. Assuming an intrinsically isothermal distribution, we find from the Flexion signal alone a velocity width of $v_c = 221 \pm 12 \text{ km/s}$ for lens galaxies of $r < 21.5$, subject to uncertainties in the intrinsic Flexion distribution.

Subject headings: galaxies: halos — galaxies: structure — gravitational lensing

1. INTRODUCTION

The past several years have seen an explosion in the analysis of weakly gravitationally lensed images of galaxies by galaxies (e.g. Brainerd, Blandford & Smail 1996; Hoekstra, Yee, & Gladders, 2004), clusters (e.g. Smail et al. 1997; Wittman, 2001; Gray et al. 2002; Taylor et al. 2004), and Large Scale Structure (e.g. Wittman et al. 2002; Hoekstra et al. 2002; Jarvis et al. 2003; Brown et al. 2003; Pen et al. 2003; Bacon et al. 2003) producing an unprecedented glimpse into the underlying matter distribution of the universe. Galaxies-galaxy lensing, in particular, has proven a fertile testbed of our understanding of structure formation.

Dynamical estimates of galaxy masses are subject to uncertainties about whether a system is relaxed, and are limited by the lack of luminous dynamical probes beyond a few tens of kpc from the center of a galaxy. Gravitational lensing techniques, on the other hand, provide an accurate way of computing the surface density of distant objects without recourse to dynamical estimates, since the distortion of images is dependent only upon the potential field of a lens and not upon either its composition or dynamics. The success of these endeavors has been such that there are a number of ongoing surveys of weak lensing fields (e.g. Wittman et al. 2002, hereafter DLS; CFHT Legacy Survey, <http://www.cfht.hawaii.edu/Science/CFHTLS-DATA/>) and instruments (e.g. Advanced Camera for Survey, Clampin et al. 2000; Dark Matter Telescope; Supernova/Acceleration Probe, Rhodes et al. 2004) largely designed around the acquisition of large high-quality lensing data. Moreover, there remains a potential bounty of information to be found in existing and ongoing survey data (e.g. SDSS, York et al. 2000; Great Observatories Origins Deep Survey, Giavalisco et al. 2004; Medium Deep Survey, Ratnatunga, Griffiths & Ostrander 1999). Given the difficulty and expense in collecting high-quality surveys of lensed galaxies it is imperative that we extract as much information as possible from them.

One of the great advantages of studying weak lensing fields is that the physics underlying gravitational lensing is well understood (see e.g. Blandford & Narayan, 1992; Kaiser & Squires, 1993; Kaiser, Squires & Broadhurst, 1995, hereafter KSB; Mellier 1999; Bartelmann & Schneider, 2001 for reviews of weak lensing). The KSB approach provides the standard for most current analyses of weak lensing, and is based upon estimating the ellipticity of a lensed galaxy as a probe of the local shear field. By measuring the ensemble properties of ellipticity and orientation for a number of sources, one can make a determination of the properties of the lens.

While the currently applied approaches have done an excellent job in estimating the matter distribution of gravitational lenses, they ultimately measure only the ellipticity of an image (the second moments), and thus potentially drop significant information from sources with significant substructure. In order to improve on this, we plan to extend the work of Goldberg & Natarajan (2002) who suggested that second order effects in gravitational lensing fields may give rise to an octopole moment in the light distribution, which expresses itself as “flexion” in the image.

The method of Goldberg & Natarajan ultimately relied on a very complicated form of the 2nd order shear operator, which made a practical inversion difficult. Instead, here we will cast this approach into a “Shapelets” formalism (Refregier, 2003; Refregier & Bacon, 2003), a novel approach to both image and lensing analysis. Rather than analyze image shapes according to their multipole moments, shapelets methodology decomposes images into combinations of Hermite polynomials. As a reminder to the reader, the reduced Hermite polynomials are the eigenfunctions of the simple harmonic oscillator in quantum mechanics, $B_n(x)$. These functions have a number of useful properties, including orthogonality and a Gaussian factor, which localizes the function.

In § 2, we begin by reviewing basic properties of the “forward” problem in weak gravitational lensing, and define our notation within the present work. We then proceed to introduce the second order term in the lensing operator, and then discuss a particularly useful approach to the second order problem using the shapelets formalism. In § 3 we discuss a

practical technique for inversion of the density gradient signal. In § 4 we provide a proof of concept by measuring the second order shear signal from Galaxy-Galaxy lensing in several DLS shear fields. We conclude with a discussion of future prospects.

2. SECOND ORDER LENSING

2.1. Review of Weak Lensing Formalism

We begin with a brief review of weak lensing theory. An excellent discussion of this material can be found in Bartelmann & Schneider (2001), from which we borrow our conventions. Imagine that we are observing a set of extended sources at an angular diameter distance, D_s which are gravitationally lensed by a mass distribution at an angular diameter distance, D_l . We thus define a dimensionless surface density, the convergence, κ , such that:

$$\kappa(\mathbf{x}) \equiv \frac{D_{ls}D_l}{D_s} \frac{4\pi G\Sigma(\vec{\theta})}{c^2}, \quad (1)$$

where Σ is the surface density of the lens, D_{ls} is the distance between lens and source and \mathbf{x} represents the image coordinates as seen by the observer (neglecting a constant coordinate transform).

The convergence may be thought of as a source term for a potential, $\psi(\theta)$, and related via a Poisson-like equation:

$$\nabla^2\psi(\mathbf{x}) = 2\kappa(\mathbf{x}), \quad (2)$$

where all gradients and divergences are calculated in two dimensions.

Since lensing conserves surface brightness, a mapping from foreground to background coordinates is sufficient to determine a background brightness map from a foreground one (or vice-versa) provided a full knowledge of the geometry of the system (cosmology plus the redshifts of the source and lens) and mass distribution of the lens. Thus, we may expand around the origin to determine a deprojection operator on a foreground light distribution, which yields the amplification matrix,

$$\mathbf{A}(\mathbf{x}) \equiv \frac{\partial\mathbf{x}'}{\partial\mathbf{x}} = \left(\delta_{ij} - \frac{\partial^2\psi(\mathbf{x})}{\partial x_i\partial x_j} \right) \equiv \begin{pmatrix} 1 - \kappa - \gamma_1 & -\gamma_2 \\ -\gamma_2 & 1 - \kappa + \gamma_1 \end{pmatrix}. \quad (3)$$

where \mathbf{x}' are the coordinates that the lensed image would have in the absence of lensing. Note that for convenience we set the origins of both the foreground and background coordinate systems to be the centers of light in their respective planes.

Equation (3) is the first term in a Taylor series expansion of the distortion operator. The term γ is a complex shear term, representing the anisotropic part of the distortion, with $\gamma = |\gamma|e^{2i\phi}$, and the real and imaginary parts being denoted with the subscripts, “1” and “2” respectively, as per convention.

If we assume that the convergence and shear field were constant along the scale of the lensed image, the brightness map of a galaxy would transform with the simple relation:

$$x'_i = A_{ij}x_j. \quad (4)$$

2.2. Expansion to 2nd Order

Of course, the field is not a constant. Thus, we may imagine expanding the field to second order such that:

$$x'_i \simeq A_{ij}x_j + \frac{1}{2}D_{ijk}x_jx_k \quad (5)$$

where

$$D_{ijk} = \frac{\partial A_{ij}}{\partial x_k} \quad (6)$$

As Kaiser (1995) has pointed out, there are a number of relationships in the derivatives of κ and γ which greatly simplify the construction of \mathbf{D} :

$$\begin{pmatrix} \kappa_{,1} \\ \kappa_{,2} \end{pmatrix} = \begin{pmatrix} \gamma_{1,1} + \gamma_{2,2} \\ \gamma_{2,1} - \gamma_{1,2} \end{pmatrix}. \quad (7)$$

Thus,

$$D_{ij1} = \begin{pmatrix} -2\gamma_{1,1} - \gamma_{2,2} & -\gamma_{2,1} \\ -\gamma_{2,1} & -\gamma_{2,2} \end{pmatrix} \quad (8)$$

$$D_{ij2} = \begin{pmatrix} -\gamma_{2,1} & -\gamma_{2,2} \\ -\gamma_{2,2} & 2\gamma_{1,2} - \gamma_{2,1} \end{pmatrix}$$

Now, let us suppose that there exists some background brightness field, $f(\mathbf{x}')$, such as the brightness of some background galaxy. Since lensing preserves surface brightness, we may write the apparent foreground brightness field as:

$$f(\mathbf{x}) = f'[\mathbf{x}'(\mathbf{x})]. \quad (9)$$

We can write the brightness as:

$$\begin{aligned} f(\mathbf{x}) &\simeq f'(\mathbf{A}\mathbf{x} + \frac{1}{2}\mathbf{D}\mathbf{x} \otimes \mathbf{x}) \\ &= f'[\mathbf{x} + (\mathbf{A} - \hat{\mathbf{I}})\mathbf{x} + \frac{1}{2}\mathbf{D}\mathbf{x} \otimes \mathbf{x}] \end{aligned} \quad (10)$$

Or, expanding as a Taylor series:

$$\begin{aligned} f(\mathbf{x}) &\simeq \left\{ 1 + \left[(A - I)_{ij}x_j + \frac{1}{2}D_{ijk}x_jx_k \right] \frac{\partial}{\partial x_i} \right. \\ &\quad \left. + \frac{1}{2} \left[(A - I)_{ik}x_k + \frac{1}{2}D_{ikl}x_kx_l \right] \left[(A - I)_{jk}x_k + \frac{1}{2}D_{jkl}x_kx_l \right] \frac{\partial^2}{\partial x_i \partial x_j} \right\} f'(\mathbf{x}) \end{aligned} \quad (11)$$

Expanding out the terms on the first line the expressions are first order in γ , and (up to) 2nd order in position, while the terms on the second line are (at least) 2nd order in position, and 2nd order in γ . If the scale on which γ varies is typically smaller than the image size, the terms on the second line will necessarily be smaller than the 2nd order contribution on the first, and thus we will consider only the first line.

Thus, in the limit of a smoothly varying, weak shear field, we have the relation:

$$f(\mathbf{x}) \simeq \left\{ 1 + \left[(A - I)_{ij}x_j + \frac{1}{2}D_{ijk}x_jx_k \right] \frac{\partial}{\partial x_i} \right\} f'(\mathbf{x}) . \quad (12)$$

2.3. Image Analysis Using Shapelets

While equation (12) defines a linear transformation on an image due to lensing, in practice it is fairly complicated to actually perform such a transformation (or the inversion) in generality. However, we may simplify this problem considerably by decomposing the image into basis coefficients.

Following Refregier & Bacon (2003), we expand the image into Reduced Hermite polynomials, or ‘‘Shapelets.’’ The light distribution, $I(x, y)$ of a galaxy is expanded as a combination of two-dimensional basis functions:

$$f(\mathbf{x}) = \sum_{n,m} f_{nm} B_{nm}(\mathbf{x}) . \quad (13)$$

where

$$B_{nm}(\mathbf{x}; \beta) = \beta^{-1} \phi_n(\beta^{-1}x_1) \phi_m(\beta^{-1}x_2) , \quad (14)$$

and where β is a scaling factor, and ϕ_n are the reduced Hermite polynomials:

$$\phi_n(x) = \left[2^n \pi^{1/2} n! \right]^{-1/2} \mathcal{H}_n(x) e^{-\frac{x^2}{2}} \quad (15)$$

such that:

$$\mathcal{H}_n'' - 2x\mathcal{H}_n' + 2n\mathcal{H}_n = 0 . \quad (16)$$

Since the lowest order polynomials resemble Gaussian light profiles, Refregier (2003) demonstrates that for typical HST images, convergence can rapidly be reached using a few $\times 10$ coefficients.

It should be noted that though this expansion is not the same as a multipole expansion, it has many similar properties. For example, an image with $f_{20} = a^2$, and $f_{02} = b^2 < a^2$ will look like an ellipse with a Gaussian radial profile. Likewise, any combinations for which $n + m$ is even produces an image which is symmetric with respect to 180 degree rotations (see, e.g. Figure 2 in Refregier, 2003). The canonical pictures of both spiral and elliptical galaxies have precisely this symmetry, and thus, it is possible that typical galaxies can be reconstructed almost exclusively from even moments.

If, taking our example from the SHO in quantum mechanics, we define:

$$\hat{p}_i \equiv \frac{\partial}{\partial x_i} ; \quad \hat{x}_i = x_i \quad (17)$$

and expand Equation 12 to first order in γ , then we get:

$$f(\mathbf{x}) \simeq \left[1 + (A - I)_{ij} \hat{x}_j \hat{p}_i + \frac{1}{2} D_{ijk} \hat{x}_j \hat{x}_k \hat{p}_i \right] f'(\mathbf{x}) \quad (18)$$

Again following Refregier & Bacon (2003), we expand our light function in Shapelets and can apply the distortion operator as a combination of raising and lowering operators. Note that we have implicitly defined our coordinates such that the β parameter used in Refregier (2003) is equal to 1. Recall,

$$\hat{x}_i = \frac{1}{\sqrt{2}}(\hat{a}_i + \hat{a}_i^\dagger) \quad \hat{p}_i = \frac{1}{\sqrt{2}}(\hat{a}_i - \hat{a}_i^\dagger) \quad (19)$$

and can operate on a Shapelet (e.g. with $i = 1$) as:

$$\hat{a}_1 |\phi_n m\rangle = \sqrt{n} |\phi_{n-1} m\rangle \quad (20)$$

$$\hat{a}_1^\dagger |\phi_n m\rangle = \sqrt{n+1} |\phi_{n+1} m\rangle \quad (21)$$

and similarly for the y-axis.

Now, the first thing to note is that with the addition of the \hat{D} operator, there are odd combinations of \hat{x} and \hat{p} , meaning that there can be coupling between $\Delta n + \Delta m = \text{odd}$ modes. Contrary to ordinary weak lensing, in which an image is lensed symmetrically around its center of light (and thus, the centroid remains fixed), second order effects will cause a shift in the center of light. We must thus compute the shift in the center of light.

Because of the inherent symmetries in the linear lensing operator, the only contribution to the centroid shift comes from the second order operator:

$$\langle x_l \rangle = \frac{1}{2} D_{ijk} \int d^2 \mathbf{x} x_l x_k x_k \frac{df'}{dx_i} \quad (22)$$

Expanding this out and integrating, we find that the center of light in the foreground will be shifted by:

$$\begin{aligned} \langle x_1 \rangle &= -\langle x_1'^2 \rangle \left(\frac{3}{2} D_{111} + D_{212} \right) - \langle x_1' x_2' \rangle (2D_{112} + D_{222}) - \langle x_2'^2 \rangle \left(\frac{1}{2} D_{122} \right) \\ \langle x_2 \rangle &= -\langle x_1'^2 \rangle \left(\frac{1}{2} D_{211} \right) - \langle x_1' x_2' \rangle (2D_{212} + D_{111}) - \langle x_2'^2 \rangle \left(\frac{3}{2} D_{222} + D_{112} \right) \end{aligned} \quad (23)$$

where the second moments of the light distribution can be computed from the foreground field (since changes in the moments from background to foreground will necessarily be 2nd order in γ , and thus negligible).

A translational shift can be given by the operator:

$$\hat{T}_i = \frac{1}{\sqrt{2}}(\hat{a}_i^\dagger - \hat{a}_i) \quad (24)$$

Combining all of this yields the following lensing operator:

$$f(\mathbf{x}) \simeq (1 + \kappa \hat{K} + \gamma_i \hat{S}_i^{(1)} + \gamma_{i,j} \hat{S}_{ij}^{(2)}) f(\mathbf{x}') \quad (25)$$

where \hat{K} is the convergence operator:

$$\hat{K} = 1 + \frac{1}{2}(\hat{a}_1^{\dagger 2} + \hat{a}_2^{\dagger 2} - \hat{a}_1^2 - \hat{a}_2^2) \quad (26)$$

and $\hat{S}_i^{(1)}$ is the linear shear operator defined by Refregier (2003):

$$\hat{S}_1^{(1)} = \frac{1}{2}(\hat{a}_1^{\dagger 2} - \hat{a}_2^{\dagger 2} - \hat{a}_1^2 + \hat{a}_2^2) \quad (27)$$

$$\hat{S}_2^{(1)} = \hat{a}_1^\dagger \hat{a}_2^\dagger - \hat{a}_1 \hat{a}_2 \quad (28)$$

It is straightforward, albeit tedious, to derive the explicit form of the second order operator, $\hat{S}^{(2)}$ from equations (18) and (22-24). We write out the explicit 2nd order transformation as:

$$S_{11}^{(2)} = \frac{1}{4\sqrt{2}} \left[-2\hat{a}_1^3 + \hat{a}_1 (4 - 2\hat{N} + 12 \langle xx \rangle) + 8 \langle xy \rangle \hat{a}_2 - 8 \langle xy \rangle \hat{a}_2^\dagger + \hat{a}_1^\dagger (6 + 2\hat{N} - 12 \langle xx \rangle) + 2\hat{a}_1^{\dagger 3} \right] \quad (29)$$

$$S_{12}^{(2)} = \frac{1}{4\sqrt{2}} \left[-8 \langle xy \rangle \hat{a}_1 + 2\hat{a}_2^3 + \hat{a}_2 (-4 + 2\hat{M} - 12 \langle yy \rangle) + \hat{a}_2^\dagger (-6 - 2\hat{M} + 12 \langle yy \rangle) - 2\hat{a}_2^{\dagger 3} + 8 \langle xy \rangle \hat{a}_1^\dagger \right] \quad (30)$$

$$S_{21}^{(2)} = \frac{1}{4\sqrt{2}} \left[-3\hat{a}_1^2\hat{a}_2 - \hat{a}_1^2\hat{a}_2^\dagger + 12 \langle xy \rangle \hat{a}_1 - \hat{a}_2^3 + \hat{a}_2 \left(3 - 2\hat{N} - 1\hat{M} + 2 \langle xx \rangle + 10 \langle yy \rangle \right) \right. \\ \left. + \hat{a}_2^{\dagger 1} \left(6 + 2\hat{N} + \hat{M} - 2 \langle xx \rangle - 10 \langle yy \rangle \right) + \hat{a}_2^{\dagger 3} - 12 \langle xy \rangle \hat{a}_1^\dagger + \hat{a}_1^{\dagger 2}\hat{a}_2 + 3\hat{a}_1^{\dagger 2}\hat{a}_2^\dagger \right] \quad (31)$$

$$S_{22}^{(2)} = \frac{1}{4\sqrt{2}} \left[-\hat{a}_1^3 - 3\hat{a}_1\hat{a}_2^2 + \hat{a}_1 \left(3 - \hat{N} - 2\hat{M} + 10 \langle xx \rangle + 2 \langle yy \rangle \right) + \hat{a}_1\hat{a}_2^{\dagger 2} + 12 \langle xy \rangle \hat{a}_2 \right. \\ \left. - 12 \langle xy \rangle \hat{a}_2^\dagger - \hat{a}_1^\dagger\hat{a}_2^2 + \hat{a}_1^\dagger \left(6 + \hat{N} + 2\hat{M} - 10 \langle xx \rangle - 2 \langle yy \rangle \right) + 3\hat{a}_1^\dagger\hat{a}_2^{\dagger 2} + \hat{a}_1^{\dagger 3} \right], \quad (32)$$

where $\hat{N}B_{nm}(x, y) = nB_{nm}(x, y)$, and similarly for \hat{M} .

Interestingly, all of the terms in the second order shear couples $\Delta n + \Delta m = \text{odd}$ coefficients, while the first term shear and convergence operators couple $\Delta n + \Delta m = 2$. In other words, we may consider only the “odd” (meaning $n+m=\text{odd}$) moments when estimating the parameters $\gamma_{i,j}$, and only the even moments ($n+m=\text{even}$) when estimating the shear γ_i , since all coefficients with n or m as odd in the background image will have an expectation value of zero. Since deviations from zero suggest a second order signal, we are not required to subtract two large modes (e.g. $f_{20} - f_{02}$), and thus add considerable noise, in order to extract a signal. We discuss a practical inversion technique in the next section.

3. PRACTICAL PARAMETER ESTIMATION

While the above relations appear fairly complicated, in reality, inversion is actually quite straightforward. Below, we describe a practical technique of inverting a set of shapelet coefficients to yield an estimate of the shear and its derivatives.

3.1. Measurement and Signal Noise

As Refregier (2003) notes, if the pixel noise is independent (e.g. Poisson), then the covariance matrix of shapelet coefficients will be simply related by:

$$V_{\mathbf{n}_1 \mathbf{n}_2} = \sigma_N^2 \delta_{\mathbf{n}_1 \mathbf{n}_2}, \quad (33)$$

where σ_N is simply the Poisson noise of the integrated signal. Though each mode has equal noise, the signal strength from the first and second order lensing signals are quite different, and it would be helpful to consider in which regime each dominates.

The approximate strength of the second order lensing signal may be inferred from equation (12). Note that all of the terms in D_{ijk} are proportional to $d\gamma/dr$. If the lens is an isothermal sphere (or any other power law relation), then $D_{ijk} \propto \gamma/R_{lens}$, where R_{lens} is the angular distance from the source to lens. Likewise, the integral of $x_j x_k \partial/\partial x_i$ over the source image will produce a term proportional to the angular scale of the image, itself. We give the “size” of a galaxy image as its semi-major axis, a_{gal} . Thus, the 2nd order lensing signal will have a strength which scales like:

$$\delta f_{nm=\text{odd}} \propto \gamma \frac{a_{gal}}{R_{lens}}, \quad (34)$$

which means that unless the source is relatively close to the lens in the image plane, measurement errors can swamp the signal. However, it is anticipated (and below, shown), that the *intrinsic* variance in this signal is significantly smaller than the variance in the shear. Moreover, in the particular regime of interest – nearby galaxy pairs, as found in galaxy-galaxy fields, this signal will be particularly well-pronounced.

It should also be noted that, in general, the observed galaxy image is convolved with a PSF. Refregier & Bacon (2003) discuss a PSF inversion technique. We do not apply the inversion in the present work, restricting ourselves to large galaxies where the impact of the PSF is small. However, we will explicitly perform a PSF inversion in a forthcoming paper. It should further be noted that inversion of the PSF gives rise to a non-diagonal covariance matrix, and we thus use the more general form of the covariance matrix in our parameter estimation below.

3.2. Inversion of the Shapelet Coefficients

In order to compute the lensing coefficients, we need to invert equation (25). In practice, this is somewhat simpler than it might initially appear, since, for example, the convergence, κ cannot be uniquely estimated from a given shear field (a constant κ value can be arbitrarily added to the reconstruction). This is known as the “mass-sheet degeneracy,” (Kaiser & Squires 1993), and, excluding this effect, we may write down a goodness of fit relation as:

$$\chi^2 \equiv \left[\mu_{n_1 m_1} - f_{n_1 m_1} + (\gamma_i \hat{S}_i^{(1)} + \gamma_{i,j} S_{ij}^{(2)}) \bar{f}_{n'_1 m'_1} \right] V_{n_1 m_1 n_2 m_2}^{-1} \left[(\mu_{n_2 m_2} - f_{n_2 m_2} + (\gamma_i \hat{S}_i^{(1)} + \gamma_{i,j} S_{ij}^{(2)}) \bar{f}_{n'_2 m'_2} \right] \quad (35)$$

where the lensing operators implicitly bring power from the primed to unprimed indices. We have defined, μ_{nm} as the “expected” source signal. For $n+m=\text{even}$, this is simply the average of the measured signal (since the universe has no preferred direction), and for $n+m=\text{odd}$, we set this to zero. Likewise, \bar{f}_{nm} is the best estimate unlensed signal. This is subtly different as, though the odd terms are still set to zero, the even terms are the observed coefficients. Since lensing (especially in galaxy-galaxy fields) is expected to be small, the best estimate of an intrinsic moment is the measured moment itself.

Because we have defined the source terms for the odd moments as zero, we may break the above expression into two separate terms:

$$\chi^{2(\text{even})} = \left[\mu_{n_1 m_1} + (\gamma_i \hat{S}_i^{(1)} - 1) f_{n'_1 m'_1} \right] V_{n_1 m_1 n_2 m_2}^{-1} \left[(\mu_{n_2 m_2} - (1 + \gamma_i \hat{S}_i^{(1)}) f_{n'_2 m'_2} \right] \quad (36)$$

$$\chi^{2(\text{odd})} = \left[f_{n_1 m_1} - \gamma_{i,j} S_{ij}^{(2)} f_{n'_1 m'_1} \right] V_{n_1 m_1 n_2 m_2}^{-1} \left[(f_{n_2 m_2} - \gamma_{i,j} S_{ij}^{(2)} f_{n'_2 m'_2} \right] \quad (37)$$

Since the first order term only lenses even moments to even moments, and the second order term only lenses even moments to odd moments, the two can be computed independently. In other words, the second-order effects represent an entirely new calculation, while the first order χ^2 can be minimized exactly as described by Refregier & Bacon (2003).

Once the gradient of the complex shear has been estimated via minimization of χ^2 , we may relate this to the gradient of the convergence using equation (7). We refer to the bending of the observed image as the estimated ‘‘Flexion’’:

$$\mathcal{F} \equiv (\tilde{\gamma}_{1,1} + \tilde{\gamma}_{2,2}) \mathbf{i} + (\tilde{\gamma}_{2,1} - \tilde{\gamma}_{1,2}) \mathbf{j}, \quad (38)$$

where $\tilde{\gamma}_{i,j}$ is the estimated inversion of the shear derivatives from the χ^2 minimization. Note that, in principle, \mathcal{F} could be used to reconstruct a convergence field. In the present worked example, however, noise plays too much of a role.

3.3. Noise

With no atmospheric or instrumental effects, the gradient estimator can be related to the true signal via the relation:

$$\mathcal{F} = \nabla \kappa \pm \sigma_{\mathcal{F},P} \pm \sigma_{\mathcal{F},S} \quad (39)$$

We have already discussed the Poisson measurement noise ($\sigma_{\mathcal{F},P}$) above. However, much like in conventional lensing, we must also take into account the intrinsic scatter in shapes amongst real galaxies.

To measure the intrinsic scatter, we observed two complementary regimes. First, we measured the shear and flexion variance in the DLS fields themselves. Secondly, we examined the shear and flexion in two clusters from the HST archive, Abell 665 and Abell 2390, and selected elliptical and spiral galaxies. We found 75 ellipticals and 53 spirals in our cluster sample which were large and bright enough to classify by eye. No classification was done on DLS galaxies.

For these samples, we measure the distribution function of ellipticity (shear) and Flexion; the results for clusters are shown in Fig. 1. We define the Flexion in units of the inverse of the semi-major of the observed galaxy. In this way, it is a dimensionless, and distance-independent measure of the shape. We find that for both ellipticals and spirals, the standard deviation in shear is relatively low, $\sigma_{\gamma,E} = 0.10$, and $\sigma_{\gamma,S} = 0.13$, respectively.

The scatter in the shear is somewhat lower than that which is normally measured. For example, in the COMBO-17 sample discussed in Brown et al. (2003), the standard deviation of the ellipticity is approximately 0.25, approximately twice as large, and consistent with the estimate from Brainerd et al. (1996). However, taking the same sample, and using only those galaxies with $r < 17$, $\sigma_{\gamma} = 0.16$. Since traditional approaches use the KSB technique to invert the PSF for small galaxies (an intrinsically noisy inversion), additional scatter is produced in the shear. Since we are interested in

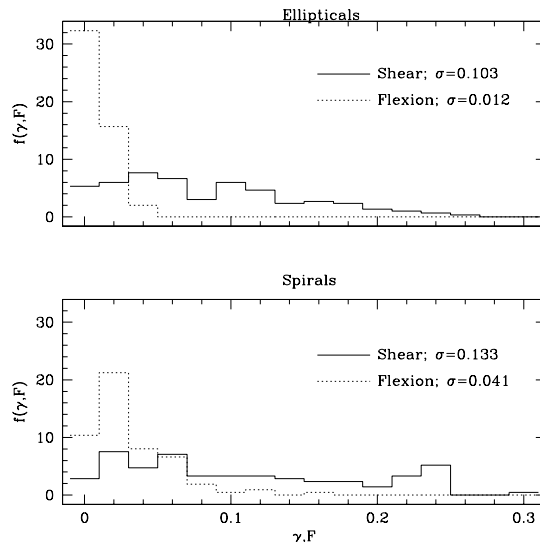


FIG. 1.— The fraction of observed galaxies with a particular measured ellipticity (solid) and flexion, $a_{gal} \times \mathcal{F}$ (dashed) from HST clusters A665, and A2390. Since lensing effects are generally small, and lensing orientation angles are randomized, we suppose this distribution to represent the intrinsic galaxy shape distribution of the background sample. Note that while the shear distribution for both spirals and ellipticals are similar, ellipticals produce a far smaller scatter in Flexion than do spirals.

the intrinsic scatter for the present work, we use our lower estimate of σ_γ . We caution, however, that, even compared to bright galaxy sample in COMBO-17, this may be a modest underestimate of the true value.

For the Flexion, we find a much larger scatter among spirals than ellipticals, with a standard deviation of $\sigma_{F,S} = 0.041$, and $\sigma_{F,E} = 0.012$, respectively. This gives the expected result that early-type galaxies are significantly more regular than late types.

Since sources with lower resolution will be harder to classify, we would like to take a typical Flexion and shear for field galaxies. Making the approximation that 60% of a randomly selected background population will be spirals (e.g. Postman & Geller 1984), we find a typical shear of $\sigma_\gamma = 0.12$, and $\sigma_F = 0.029$. These results have a similar to that found in the well resolved (but morphologically unclassified) sample from the DLS, yielding, $\sigma_{\gamma,DLS} = 0.14$, and $\sigma_{F,DLS} = 0.04$.

Using the HST estimates, we may perform a simple estimate of signal to noise. For the first order signal, we find:

$$\left(\frac{S}{N}\right)^{(1)} \simeq \frac{\gamma}{0.12} \quad (40)$$

And, likewise, for the flexion signal,

$$\left(\frac{S}{N}\right)^{(2)} \simeq \frac{\gamma/R_{lens}}{0.029/a_{gal}}, \quad (41)$$

since for an isothermal sphere

$$\begin{aligned} \frac{d\kappa}{dr} &= -\frac{d\gamma}{dr} \\ &= \frac{\gamma}{R_{lens}} \end{aligned} \quad (42)$$

since $\gamma \propto 1/R$.

The signals from first and second order effects will be comparable if:

$$R_{lens} \simeq 4.1 a_{gal} \quad (43)$$

Thus, at modest separations, the signal to noise from the second order signal will be comparable to the traditional shear signal. This ratio will rise to a factor of 10 if the background sample consists entirely of ellipticals. Moreover, it provides an entirely new source of information, as it is a direct estimator of the underlying surface density of the lens.

3.4. Parameter Estimation with a Nearly Circular PSF

In practice, we do not generally directly estimate either the shear or the flexion directly from averages over the ellipticities. Even a perfectly circular PSF will alter the value, but not the orientation, of the estimated parameters. As a result, we will generally wish to consider only the relative orientation of the shear or the flexion with respect to the candidate lens.

In practice, this means measuring the Flexion and shear of a large number of background sources which separated from their respective lenses by a fixed range of distances. The distribution function of the relative orientation angles of both Flexion and shear and then computed. In the absence of lensing, we would assume these distributions would be drawn from a uniform prior. However, lensing will tend to orient the shear perpendicular to the lens, and the Flexion toward the lens.

We must thus relate the distribution function of relative orientation angles, P_ϕ , to the induced shear (in first order) or flexion (in second order) of the lens. Traditional galaxy-galaxy lensing inversion techniques (Brainerd et al. 1996) yield a relation:

$$P_\phi^{(1)} = \frac{2}{\pi} [1 - \langle \gamma \rangle \cos 2\phi_1 \langle e^{-1} \rangle] \quad (44)$$

over the domain $\phi_1 = [0, \pi/2]$. The normalization term, $\langle e^{-1} \rangle$ is exceedingly noisy, and can be unstable for small values of ellipticity. Thus, using the parametric model of Brainerd et al. (1996):

$$P(e) \propto e \exp -A \times e, \quad (45)$$

Using this relation, we find $\langle e^{-1} = 14.4 \rangle$ from the σ_γ discussed above. Note, again, that this is somewhat larger than the value of 8 found by Brainerd et al. (1996).

A virtually identical derivation will yield a relation between the orientation of the flexion:

$$P_\phi^{(2)} = \frac{1}{\pi} \left[1 - \langle A \frac{d\kappa}{dr} \rangle \cos \phi_2 \langle (a_{gal} \mathcal{F})^{-1} \rangle \right]. \quad (46)$$

Assuming a similar shape to the shear and Flexion distribution function, and using the ratio $\sigma_\gamma/\sigma_F = 4.1$ found above, our estimate of the flexion deviation is, $\langle (a_{lens} \mathcal{F})^{-1} \rangle \simeq 59$, over $\phi_2 = [0, \pi]$.

4. PROOF OF CONCEPT: THE DLS

As a proof of concept of this technique, we apply it to the Deep Lens Survey (DLS). The DLS (Wittman et al. 2002) is an ongoing deep optical survey of 7×4 square degree fields, taken on the NOAO 4m Blanco and Mayall telescopes. Each field will have an integrated 18ks exposure in the R band, and 12 ks each in the B, V, and z' bands. For the present test, we use only R band photometry. While the DLS is designed for measurements of lensing from Large Scale Structure, it is also ideally suited for our purposes, as the fields are selected around otherwise empty regions in the sky, and thus the primary lensing potential will come from galaxies or large-scale structure only.

We looked at all 17 of the DLS subfields from the first three public data releases, amounting to a total area of approximately 5.4 square degrees. We select as potential lensed sources only those galaxies which have $21.5 < r < 23$, and which have semi-major axes $A > 0.9''$, since objects significantly smaller than that are not well-resolved into high order shapelets. This is a far more conservative cut than on a shallower sample than that used by Brainerd et al. (1996), however, we wish to re-emphasize that our goal in this work is to demonstrate the detectability of the Flexion signal. Thus, taking as potential lenses those galaxies with $18 < r < 21.5$. In total, we found 4833 potential pairs (similar to the number found in the Brainerd et al. 1996 sample) with separations less than $60''$ over 17 subfields.

We then decompose all background galaxies into shapelet coefficients as described above, and estimate the best fit Flexion and shear by minimization χ^2 as in equation (37). Since seeing produces a significant reduction in the magnitude of the shear and Flexion, we use only the orientation angles.

The distribution of relative orientation angles for pairs with separation less than $16''$ and greater than $5''$ is shown in Fig. 2, along with a best fit curve representing a shear of $\gamma = 0.006 \pm 0.006$ and $\mathcal{F} = 0.0027 \pm 0.0012''^{-1}$. We use a KS test in all cases to determine best fit parameters. Since the shear and Flexion should be preferentially aligned

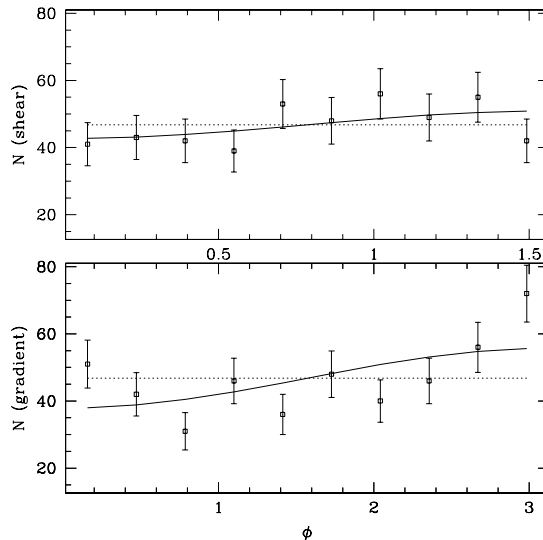


FIG. 2.— The distribution of relative orientation angles of the shear (top panel) and flexion (bottom panel) with respect to a potential lens within a separation of $16''$. The lines indicate a best fit to equations (44) and (46), of $\gamma = 0.006 \pm 0.006$ and $d\kappa/dr = 0.0027 \pm 0.0012$.

either perpendicular (shear), or toward (Flexion) the source, a rotation of 45 degrees for shear and 90 degrees for Flexion (known, hereafter, as the “B-field signal”) should produce an entirely random signal. Applying these rotations to each observed source and computing the corresponding shear and Flexion produces a means of normalizing the error bars for our sample, and checking for consistency.

For example, if we divide a given sample into N_{bin} bins of lens-source separation, then we expect that the B-field terms will yield a signal with a $\chi^2 = N_{bin} - 1$, with the errorbars in each bin being proportional to $\sqrt{rN_i}$, the number of galaxies within that bin. Moreover, since the errorbars associated with the B-field should be the same as for the E-field, we may use this test as a means of normalising the E-field errorbars. We linearly correct extend the B error bars (initially assumed to be Poisson noise) such that the reduced χ^2 is 1. It should be noted that this produces approximately a 10% correction in both the Flexion and Shear errorbars from those based on an analytic estimate of uniformly sampled orientation angles.

This appears to be assuming that there is no systematic error contribution to B; however, we are simply applying a useful fiction to obtain error bars for E that *contain* the systematic error contribution. The method does not explicitly find the level of this systematic error in B, but accounts for the systematic and statistical errors when quoting an E error.

We then determine an average radial profile for both terms. We plot the average cumulative shear (measured within a disk from separations of $5''$ to r) for both terms in Fig. 3.

The radial profiles represent cumulative estimates of the shear and flexion, and thus the errorbars are strongly coupled within a given plot. At highest significance (around $10''$ for the shear, and $20''$ for the flexion), the shear and flexion result in a 1 and 2σ detection, respectively. The shear estimates are also consistent with estimates from other researchers, notably Brainerd et al. (1996) who find a shear of 0.0055 for separations of $R_{lens} < 20''$.

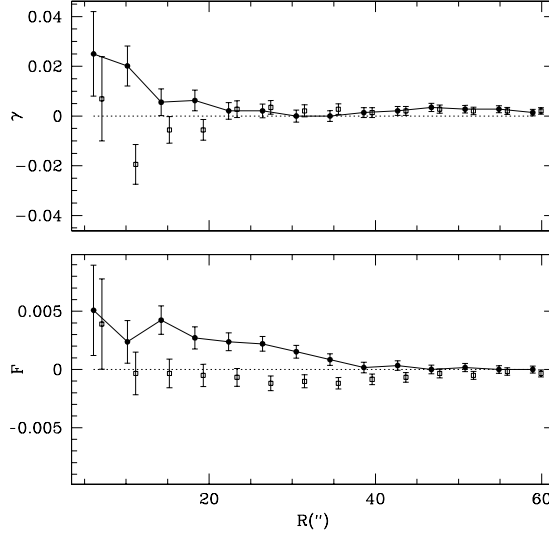


FIG. 3.— The cumulative estimate of the shear (top panel) and the flexion (bottom panel), of the first three releases from the DLS. Each solid point represents the integrated (from $R_{gal} = 5''$) E-field shear or flexion as described in the text. Note that the errorbars on each are strongly correlated. The figure is plotted such that positive shear represents source galaxies aligned tangentially to the lens, and positive values of the flexion actually represent *decreasing* surface density as a function of radius. The squares represent the B-field (rotated) signal, and are consistent with no signal. This cross-signal measurement demonstrates that our observed signal could not arise randomly.

In order to fit the data to physical parameters, we select a simple isothermal sphere model for the lens, and assume that all lenses are drawn from the same population. We then expect the relation (Bartelmann & Schneider 2001):

$$|\gamma| = \frac{2\pi}{R_{lens}} \frac{v_c^2}{c^2} \frac{D_{ls}}{D_s}, \quad (47)$$

and

$$\left| \frac{d\kappa}{dr} \right| = \frac{2\pi}{R_{lens}^2} \frac{v_c^2}{c^2} \frac{D_{ls}}{D_s}, \quad (48)$$

where D_{ls} is the angular diameter distance from source to the lens. We set this ratio to be 0.5 for our discussion since lensing signals are typically maximized around this ratio (e.g. Bartelmann & Schneider 2003), and will normalize the results to this value. Note that an error in this ratio is systematic, as it effects both our model from the flexion and from the shear identically.

We fit the isothermal sphere model in Fig. 4. Note that we may fit a velocity for either the shear or flexion estimate. For the shear, we find a fit of $(v_c = 107^{+24}_{-32} km/s)(D_s/D_{ls}/0.5)^{0.5}$, and for the flexion $v_c = (209^{+12}_{-13} km/s)(D_s/D_{ls}/0.5)^{0.5}$. These two fits may be combined to provide a best fit of $(201 \pm 11 km/s)(D_s/D_{ls}/0.5)^{0.5}$. While here we are quoting only the random error, there may also be a systematic error based on errors in the assumed distribution function of ellipticities and flexions. The shear estimate produces a significantly lower velocity than that found by Brainerd et al. (1996; 220 km/s), though the two estimates straddle the lower velocity estimate of 135 km/s found by Hoekstra et al. (2004) in the Red Cluster Survey. Nevertheless, it should be noted that the shear and Flexion estimate within our own sample are not statistically consistent. There are several possibilities.

First, an isothermal sphere may not be the best model. Consider a circularly symmetric power-law density field,

$$\kappa(r) = Ar^{-\eta}, \quad (49)$$

where $\eta = 1$ for an isothermal sphere. The Flexion for such a lens will be:

$$|\mathcal{F}| = A\eta r^{-\eta-1} \quad (50)$$

Likewise, symmetry dictates that the shear is:

$$|\gamma| = \bar{\kappa}(r) - \kappa(r) = \frac{\eta}{2-\eta} \kappa(r) \quad (51)$$

Thus:

$$\left| \frac{\mathcal{F}}{\gamma} \right| = \frac{2-\eta}{r} \quad (52)$$

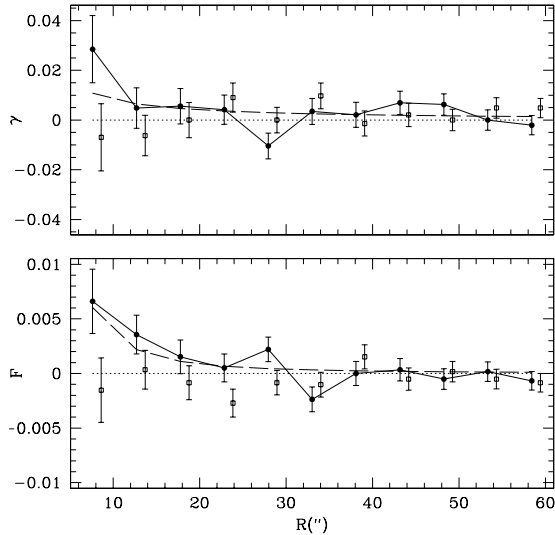


FIG. 4.— As in the previous figure, we plot the estimates of the shear and flexion of galaxies from the DLS. However, here, we plot the estimate of the differential shear from annuli of $5''$. We then fit the curves to an isothermal sphere, as described in the text. Using shear, we find $v_c = 109$ km/s., while using Flexion, we find $v_c = 221$ km/s. Again, the squares show the results of rotating the sources by 45 degrees for shear and 90 degrees for Flexion.

Thus, Flexion which indicates a very high velocity dispersion compared to the shear may, in fact, be indicative of an $\eta < 1$. In other words, such a discrepancy may be caused by a density distribution dropping off more slowly than isothermal.

Secondly, and more likely, recall that though the statistical significance of the Flexion signal can be determined internally from the data, the normalization of the signal must be estimated from the intrinsic distribution, in the case of a KS test. However, if we've overestimated the intrinsic variance of the Flexion then we will overestimate the Flexion as well. Consider that for fixed distribution of orientation angles, the normalizations of the curves may be related as:

$$\frac{v_{c, Flexion}^2}{v_{c, shear}^2} \propto \frac{\sigma_F}{\sigma_\gamma} \quad (53)$$

Thus, the two estimates may be reconciled if the ratio of σ_F/σ_γ is reduced by a factor of $(107/221)^2 = 0.23$. If this is the sole source of the discrepancy, then the Flexion may dominate the signal over shear on larger scales than originally suggested by equation 43, yielding the new relation:

$$R_{lens, equality} \simeq 17.8 a_{gal} \quad (54)$$

as the crossover scale between Flexion dominance and shear dominance.

5. FUTURE PROSPECTS

We believe that we have convincingly laid out and demonstrated the feasibility of interpreting new information from weak lensing fields by extending that analysis to second order. However, the present work leads to a number of additional areas of investigation both theoretical and observational.

First, the present work does not incorporate inversion of the Point Spread Function. It is therefore clear that we are presently unable to extract a significant signal from galaxies which are on order the same size as the PSF. As a result, we are forced to remove many potentially lensed galaxies from our sample despite the fact that information could be potentially extracted from them. We will address this issue in future work.

Secondly, the present work has actually thrown away some information with regards to measurements of the shear derivatives. Since we have four derivatives, and reduce that data to a 2-vector (\mathcal{F}), we have, in essence, thrown away information. In principle, those derivatives could yield, in addition to $d\kappa/dr$, a measurement of the variations of, say, the shear as a function of radius. Since for an isothermal sphere, these numbers are identical (up to a minus sign), this could potentially be an important test for isothermality.

As a complimentary effort, we will apply this technique to space-based data. Of particular use are the Medium Deep Survey (Ratnatunga, Griffiths, & Ostrander 1999) and GOODS (Giavalisco et al. 2004), which will provide the opportunity to measure more precisely the intrinsic distribution of flexions in background galaxies. Moreover, since the PSF is much smaller, we will be able to directly measure the component of the shear and flexion parallel to the lens-source displacement.

In summary, we have detected the second-order lensing effect, “flexion”. This effect will be of great value on its own and in conjunction with first-order lensing, in order to measure the properties of galaxy halos; it affords direct, local information on the gradient of the halo density.

DMG acknowledges support from NSF grant AST-0205080, as well as David Wittman for a number of useful correspondences, and Fiona Hoyle and Tereasa Brainerd for helpful conversations. DJB is supported by a PPARC Postdoctoral Fellowship.

REFERENCES

- Bacon, D., Massey, R.J., Refregier, A.R., & Ellis, R.S., 2003, MNRAS 344, 673
 Bartelmann, M. & Schneider, P., 2001, Physics Reports, 340, 291
 Bertin, E. & Arnouts, S., 1996, A&AS 117, 393
 Blandford, R.D., & Narayan, R., 1992, ARA&A, 30, 311
 Brainerd, T.G., Blandford, R.D. & Smail, I., 1996, ApJ 466, 623
 Brown, M.L., Taylor, A.N., Bacon, D.J., Gray, M.E., Dye, S., Meisenheimer, K. & Wolf, C., 2003, MNRAS 341, 100
 Clampin, M., et al. 2000, SPIE 4013, 344 (ACS)
 Giavalisco, M. et al. 2004, ApJL 600, 93 (GOODS)
 Goldberg, D.M. & Natarajan, P., 2002, ApJ 564, 65
 Gray, M.E., Taylor, A.N., Meisenheimer, K., Dye, S., Wolf, C., & Thommes, E., 2002, ApJ 568, 141
 Hoekstra, H., Yee, H.K.C., Gladders, M.D., Barrientos, L.F., Hall, P.B., & Infante, L., 2002, ApJ 572, 55
 Hoekstra, H., Yee, H.K.C., & Gladders, M.D. 2004, ApJ, 606, 67
 Jarvis, M., Bernstein, G.M., Fischer, P., Smith, D., Jain, B., Tyson, J.A. & Wittman, D, 2003, AJ 125, 1014
 Kaiser, N., 1995, ApJ 439, L1
 Kaiser, N. & Squires, G. 1993, ApJ 404, 441
 Kaiser, N., Squires, G., & Broadhurst, T., 1995, ApJ 449, 460
 Mellier, Y. 1999, ARA&A 37, 127
 Pen, U.-L., Lu., T., van Waerbeke, L. & Mellier, Y., 2003, MNRAS 346, 994
 Postman, M. & Geller, M. J. 1984, ApJ 281, 95
 Ratnatunga, K.V., Griffiths, R.E., & Ostrander, E.J., 1999, AJ 118, 86
 Refregier, A., 2003, MNRAS 338, 35
 Refregier, A. & Bacon, D., 2003, MNRAS 338, 48
 Rhodes, J. et al. 2004, APh 20, 377
 Smail, I., Ellis, R.S., Dressler, A., Couch, W.J., Oemler, A., Sharples, R.M. & Butcher, H., 1997, ApJ 479, 70
 Taylor, A.N., Bacon, D.J., Gray, M.E., Wolf, C., Meisenheimer, K., Dye, S. Borch, A., Kleinheinrich, M., Kovacs, Z., & Wisotzki, L., 2004, submitted to MNRAS; astro-ph/0402095
 Wittman, D. 2001, ApJL 557, L89
 Wittman, D. et al., 2002, SPIE, 4836, 73